Prediction of Respiratory Motion Using A Statistical 4D Mean Motion Model

Jan Ehrhardt[1], René Werner[1], Alexander Schmidt–Richberg[1], and Heinz Handels[1]

Department of Medical Informatics, University Medical Center Hamburg–Eppendorf, Germany, j.ehrhardt@uke.uni-hamburg.de

Abstract. In this paper we propose an approach to generate a 4D statistical model of respiratory lung motion based on thoracic 4D CT data of different patients. A symmetric diffeomorphic intensity–based registration technique is used to estimate subject–specific motion models and to establish inter–subject correspondence. The statistics on the diffeomorphic transformations are computed using the Log–Euclidean framework. We present methods to adapt the genererated statistical 4D motion model to an unseen patient–specific lung geometry and to predict individual organ motion. The prediction is evaluated with respect to landmark and tumor motion. Mean absolute differences between model–based predicted landmark motion and corresponding breathing–induced landmark displacements as observed in the CT data sets are 3.3 ± 1.8 *mm* considering motion between end expiration to end inspiration, if lung dynamics are not impaired by lung disorders.
The statistical respiratory motion model presented is capable of providing valuable prior knowledge in many fields of applications. We present two examples of possible applications in the fields of radiation therapy and image guided diagnosis.

1 Introduction

Respiration causes significant motion of thoracical and abdominal organs and thus is a source of inaccuracy in image guided interventions and in image acquisition itself. Therefore, modeling and prediction of breathing motion has become an increasingly important issue within many fields of application, e.g in radiation therapy [1].

Based on 4D images, motion estimation algorithms enable to determine patient–specific spatiotemporal information about movements and organ deformation during breathing. A variety of respiratory motion estimation approaches have been developed in the last years, ranging from using simple analytical functions to describe the motion over landmark–, surface– or intensity–based registration techniques [2, 3] to biophysical models of the lung [4]. However, the computed motion models are based on individual 4D image data and their use is usually confined to motion analysis and prediction of an individual patient.

The key contribution of this article is the generation of a *statistical* 4D inter–individual motion model of the lung. A symmetric diffeomorphic non–linear

intensity–based registration algorithm is used to estimate lung motion from a set of 4D CT images from different patients acquired during free breathing. The computed vector motion fields are transformed into a common coordinate system and a 4D mean motion model (4D–MMM) of the respiratory lung motion is extracted using the Log–Euclidean framework [5] to compute statistics on the diffeomorphic transformations. Furthermore, methods are presented to adapt the computed 4D–MMM to the patient's anatomy in order to predict individual organ motion without 4D image information. We perform a quantitative in–depth evaluation of the model–based prediction accuracy for intact and impaired lungs and two possible applications of the 4D–MMM in the fields of radiation therapy and image guided diagnosis are shown.

Few works that deal with the development of statistical lung motion models have been published. Some approaches exist for the generation of 3D lung atlases [6], or the geometry–based simulation of cardiac and respiratory motions [7]. First steps towards an average lung motion model generated from different patients were done by Sundaram et al. [8], but their work focuses on 2D+t lung MR images and the adaptation of the breathing model to a given patient has not been addressed. First methods for building inter–patient models of respiratory motion and the utilization of the generated motion model for model–based prediction of individual breathing motion were presented in [9] and [10]. This paper is an extension of [10] with regard to the methodology and the quantitative evaluation. In [9] motion models were generated by applying a Principal Component Analysis (PCA) to motion fields generated by a surface–based registration in a population of inhale–exhale pairs of CT images. Our approach is different in all aspects: the registration method, the solution of the correspondance problem, the spatial transformation of motion fields, and the computation of statistics of the motion fields. Furthermore, we present a detailed quantitative evaluation of a model based prediction for intact and impaired lungs. This offers interesting insights into the prediction accuracy to be expected depending on size and position of lung tumors.

2 Method

The goal of our approach is to generate a statistical model of the respiratory lung motion based on a set of N_p thoracic 4D CT image sequences. Each 4D image sequence is assumed to consist of N_j 3D image volumes $I_{p,j} : \Omega \rightarrow \mathbb{R}$ ($\Omega \subset \mathbb{R}^3$), which are acquired at corresponding states of the breathing cycle. This correspondance is ensured by the applied 4D image reconstruction method [11] and therefore, a temporal alignment of the patient data sets is not necessary.

Our method consists of three main steps: First, the subjectspecific motion is estimated for each 4D image sequence by registering the 3D image frames. In a second step, an average shape and intensity model is generated from the CT images. In the last step, the average shape and intensity model is used as anatomical reference frame to match all subject-specific motion models and to build an average intersubject model of the respiratory motion.

Image registration is required in all three steps. We use a non–linear, intensity–based, diffeomorphic registration method as described in the next section. The three steps to generate the statistical model of the respiratory motion are detailed in Sect. 2.2. The utilization of the 4D–MMM for motion predicition is presented in Sect. 2.3.

2.1 Diffeomorphic image registration

Diffeomorphic mappings $\boldsymbol{\varphi} : \Omega \rightarrow \Omega$, $(\boldsymbol{\varphi} \in Diff(\Omega),\ \Omega \subset \mathbb{R}^d)$ guarantee that the topology of the transformed objects is preserved and are therefore used in computational anatomy to analyze and characterize the biological variability of human anatomy [12]. A practical approach for fast diffeomorphic image registration was recently proposed in [13] by constraining $\boldsymbol{\varphi}$ to a subgroup of diffeomorphisms. Here, diffeomorphisms are parametrized by a stationary velocity field $\boldsymbol{v}$, and the diffeomorphic transformation $\boldsymbol{\varphi}$ is given by the solution of the *stationary* flow equation at time $t = 1$ [5]:

$$\frac{\partial}{\partial t}\phi(\boldsymbol{x}, t) = \boldsymbol{v}(\phi(\boldsymbol{x}, t)) \text{ and } \phi(\boldsymbol{x}, 0) = \boldsymbol{x}. \tag{1}$$

The solution of eq. (1) is given by the group exponential map $\boldsymbol{\varphi}(\boldsymbol{x}) = \phi(\boldsymbol{x}, 1) = \exp(\boldsymbol{v}(\boldsymbol{x}))$ and the significant advantage of this approach is that these exponentials can be computed very efficiently (see [5] for details).

The problem of image registration can now be understood as finding a parametrizing velocity field $\boldsymbol{v}$, so that the diffeomorphic transformation $\boldsymbol{\varphi} = \exp(\boldsymbol{v})$ minimizes a distance $\mathcal{D}$ between a reference image I_0 and the target image I_j with respect to a desired smoothness $\mathcal{S}$ of the transformation: $\mathcal{J}[\boldsymbol{\varphi}] = \mathcal{D}[I_0, I_j; \boldsymbol{\varphi}] + \alpha\mathcal{S}[\boldsymbol{\varphi}]$. Using $\mathcal{S}[\boldsymbol{\varphi}] = \int_\Omega \|\nabla \boldsymbol{v}\|^2 d\boldsymbol{x}$ (with $\boldsymbol{\varphi} = \exp(\boldsymbol{v})$) as regularization scheme, the following iterative registration algorithm can be derived:

Algorithm 1 Symmetric diffeomorphic registration

Set $\boldsymbol{v}^0 = 0$, $\boldsymbol{\varphi} = \boldsymbol{\varphi}^{-1} = Id$ and $k = 0$
repeat
Compute the update step $\boldsymbol{u} = \frac{1}{2}\left(\boldsymbol{f}_{I_0, I_j \circ \boldsymbol{\varphi}} - \boldsymbol{f}_{I_j, I_0 \circ \boldsymbol{\varphi}^{-1}}\right)$
Update the velocity field and perform a diffusive regularization:

$$\boldsymbol{v}^{k+1} = (Id - \tau\alpha\boldsymbol{\Delta})^{-1}\left(\boldsymbol{v}^k + \tau\boldsymbol{u}\right) \tag{2}$$

Calculate $\boldsymbol{\varphi} = \exp(\boldsymbol{v}^{k+1})$ and $\boldsymbol{\varphi}^{-1} = \exp(-\boldsymbol{v}^{k+1})$
Let $k \leftarrow k + 1$
until $\|\boldsymbol{v}^{k+1} - \boldsymbol{v}^k\| < \epsilon$ or $k \geq K_{max}$

The update field $\boldsymbol{u}$ is calculated in an inverse consistent form to assure source to target symmetry. The force term $\boldsymbol{f}$ is related to $\mathcal{D}$ and is chosen to be:

$$\boldsymbol{f}_{I_0, I_j \circ \boldsymbol{\varphi}}(\boldsymbol{x}) = -\frac{(I_0(\boldsymbol{x}) - (I_j \circ \boldsymbol{\varphi})(\boldsymbol{x}))\, \nabla (I_j \circ \boldsymbol{\varphi})(\boldsymbol{x})}{\|\nabla (I_j \circ \boldsymbol{\varphi})(\boldsymbol{x})\|^2 + \kappa^2 (I_0(\boldsymbol{x}) - (I_j \circ \boldsymbol{\varphi})(\boldsymbol{x}))^2} \tag{3}$$

with κ^2 being the reciprocal of the mean squared spacing. Eq. (2) performs the update of the velocity field $\boldsymbol{v}$, where τ is the step width. The term $(Id - \tau\alpha\boldsymbol{\Delta})^{-1}$ is related to the diffusive smoother $\mathcal{S}$ and can be computed efficiently using additive operator splitting (AOS).

We have chosen this diffeomorphic registration approach because of three reasons: In the context of the motion model generation, it is important to ensure that the calculated transformations are symmetric and diffeomorphic because of the multiple usage of inverse transformations. The second reason is related to runtime and memory requirements: due to the size of the 4D CT images diffeomorphic registration algorithms using non–stationary vector fields, e.g. [14], are not feasible. Third, the representation of diffeomorphic transformations by stationary vector fields provides a simple way for computing statistics on diffeomorphisms via vectorial statistics on the velocity fields.

For a diffeomorphism $\boldsymbol{\varphi} = \exp(\boldsymbol{v})$, we call the velocity field $\boldsymbol{v} = \log(\boldsymbol{\varphi})$ the logarithm of $\boldsymbol{\varphi}$. Remarkably, the logarithm $\boldsymbol{v} = \log(\boldsymbol{\varphi})$ is a simple 3D vector field and this allows to perform vectorial statistics on diffeomorphisms, while preserving the invertibility constraint [15]. Thus, the Log-Euclidean mean of diffemorphisms is given by averaging the parametrizing velocity fields:

$$\bar{\boldsymbol{\varphi}} = \exp\left(\frac{1}{N}\sum_i \log(\boldsymbol{\varphi}_i)\right). \tag{4}$$

The mean and the distance are inversion-invariant, since $\log(\boldsymbol{\varphi}) = -\log(\boldsymbol{\varphi}^{-1})$. Even though the metric linked to this distance is not translation invariant, it provides a powerful framework where statistics can be computed more efficiently than in the Riemannian distance framework. For a more detailed introduction to the mathematics of the diffeomorphism group and the associated tangent space algebra, we refer to [5] and the references therein.

2.2 Generation of a 4D mean motion model

In the first step, we estimate the intra–patient respiratory motion for each 4D image sequence by registering the 3D image frames. Let $I_{p,j} : \Omega \to \mathbb{R}$ ($\Omega \subset \mathbb{R}^3$) be the 3D volume of subject $p \in \{1, \ldots, N_p\}$ acquired at respiratory state $j \in \{0, \ldots, N_j - 1\}$. Maximum inhale is chosen as reference breathing state and the diffeomorphic transformations $\boldsymbol{\varphi}_{p,j} : \Omega \to \Omega$ are computed by registering the reference image $I_{p,0}$ with the target images $I_{p,j}$, $j \in \{1, \ldots, N_j - 1\}$. In order to handle discontinuities in the respiratory motion between pleura and rib cage, lung segmentation masks are used to restrict the registration to the lung region by computing the update field only inside the lung (see [3] for details).

In order to build a statistical model of respiratory motion, correspondence between different subjects has to be established, i.e. an anatomical reference frame is necessary. Therefore, the reference images $I_{p,0}$ for $p = 1, \ldots, N_p$ are used to generate an average intensity and shape atlas $\bar{I}_0$ of the lung in the reference breathing state by the method described in [10]. This 3D atlas image $\bar{I}_0$ is now used as reference frame for the statistical lung motion model. Each patient–specific reference image $I_{p,0}$ is mapped to the average intensity and shape atlas $\bar{I}_0$ by an affine alignment and a subsequent diffeomorphic registration.

Let $\boldsymbol{\psi}_p$ be the transformation between the reference image $I_{p,0}$ of subject p and the atlas image $\bar{I}_0$. Since the intra–subject motion models $\boldsymbol{\varphi}_{p,j}$ are defined in the anatomical spaces of $I_{p,0}$, we apply a coordinate transformation

$$\tilde{\boldsymbol{\varphi}}_{p,j} = \boldsymbol{\psi}_p \circ \boldsymbol{\varphi}_{p,j} \circ \boldsymbol{\psi}_p^{-1} \tag{5}$$

to transfer the intra–subject deformations into the atlas coordinate space. Such a coordinate transformation accounts for the differences in the coordinate systems of subject and atlas due to misalignment and size/shape variation and eliminates subject–specific size, shape and orientation information in the deformation vectors. This enables the motion fields of each of the subjects to be compared directly quantitatively and qualitatively and the 4D–MMM is generated by calculating the Log-Euclidean mean $\bar{\boldsymbol{\varphi}}_j$ of the mapped transformations for each breathing state j:

$$\bar{\boldsymbol{\varphi}}_j = \exp\left(\frac{1}{N_p}\sum_p \log\left(\tilde{\boldsymbol{\varphi}}_{p,j}\right)\right) = \exp\left(\frac{1}{N_p}\sum_p \log\left(\boldsymbol{\psi}_p \circ \boldsymbol{\varphi}_{p,j} \circ \boldsymbol{\psi}_p^{-1}\right)\right). \tag{6}$$

The method proposed in [16] was used to compute the logarithms $\log\left(\tilde{\boldsymbol{\varphi}}_{p,j}\right)$.

The resulting 4D–MMM consists of an average lung image $\bar{I}_0$ for a reference state of the breathing cycle, e.g. maximum inhalation, and a set of motion fields $\bar{\boldsymbol{\varphi}}_j$ describing an average motion between the respiratory state j and the reference state (Fig. 1).

2.3 Utilization of the 4D–MMM for individual motion prediction

The 4D–MMM generated in section 2.2 can be used to predict respiratory lung motion of a subject s even if no 4D image information is available. Presuming a 3D image $I_{s,0}$ acquired at the selected reference state of the breathing cycle is available, the 4D–MMM is adapted to the individual lung geometry of subject s by registering the average lung atlas $\bar{I}_0$ with the 3D image $I_{s,0}$. The resulting transformation $\boldsymbol{\psi}_s$ is used to apply the coordinate transformation eq. 5 to the mean motion fields $\bar{\boldsymbol{\varphi}}_j$ in order to obtain the model–based prediction of the subject–specific lung motion: $\hat{\boldsymbol{\varphi}}_{s,j} = \boldsymbol{\psi}_s^{-1} \circ \bar{\boldsymbol{\varphi}}_j \circ \boldsymbol{\psi}_s$.

However, two problems arise. First, breathing motion of different individuals varies significantly in amplitude [1]. Therefore, motion prediction using the mean amplitude will produce unsatisfying results. To account for subject–specific motion amplitudes, we propose to introduce additional information by providing the

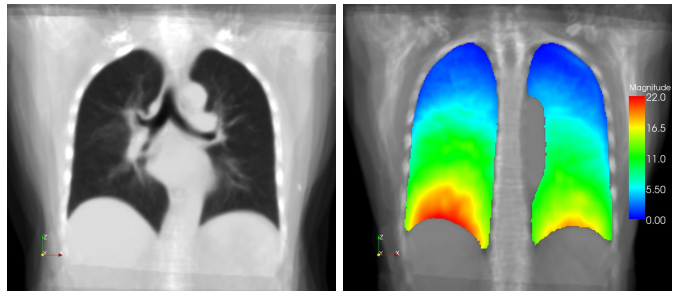

(a) (b)

Fig. 1. Visualization of average lung model $\bar{I}_0$ (a) and magnitude of mean deformation $\bar{\varphi}_j$ between end inspiration and end expiration (b). The average deformation model shows a typical respiratory motion pattern. Different windowing and leveling functions are used to accentuate inner/outer lung structures.

required change in lung air content ΔV_{air}. Even without 4D-CT data, this information can be acquired by spirometry measurements. Thus, we search a scaling factor λ so that the air content of the transformed reference image $I_{s,0} \circ \lambda \hat{\varphi}_{s,j}^{-1}$ is close to the air content $V_{air}(I_{s,0}) + \Delta V_{air}$. In order to ensure that the scaled motion field is diffeomorphic, the scaling is performed in the Log–Euclidean. To determine the correct scaling factor λ, a binary search strategy is applied and the air content is computed using the method described in [17]. ΔV_{air} can be regarded as a parameter that describes the depth of respiration. In general, other measurements can also be used to calculate appropriate scaling factors, e.g. the amplitude of the diaphragm motion.

Further, a second problem arises when predicting individual breathing motion of lung cancer patients. Lung tumors will impair the atlas–patient registration because there is no corresponding structure in the atlas. This leads to distortions in ψ_s near the tumor region and consequently the predicted motion fields $\hat{\varphi}_{s,j}$ are affected. Therefore, we decided to compute ψ_s by registering lung segmentation masks from atlas and subject s and by omitting the inner lung structures.

3 Results

To capture the respiratory motion of the lung, 18 4D CT images were acquired using a 16–slice CT scanner operating in cine-mode. The scanning protocol and optical–flow based reconstruction method was described in [11]. The spatial resolution of the reconstructed 4D CT data sets is between $0.78 \times 0.78 \times 1.5mm^3$ and $0.98 \times 0.98 \times 1.5mm^3$. Each data set consists of 3D CT images at 10 to 14 preselected breathing phases. Due to computation times, in this study we use the following 4 phases of the breathing cycle: end inspiration (EI), 42% exhale (ME), end expiration (EE) and 42% inhale (MI). A clinical expert delineated left and right lung and the lung tumors in the images.

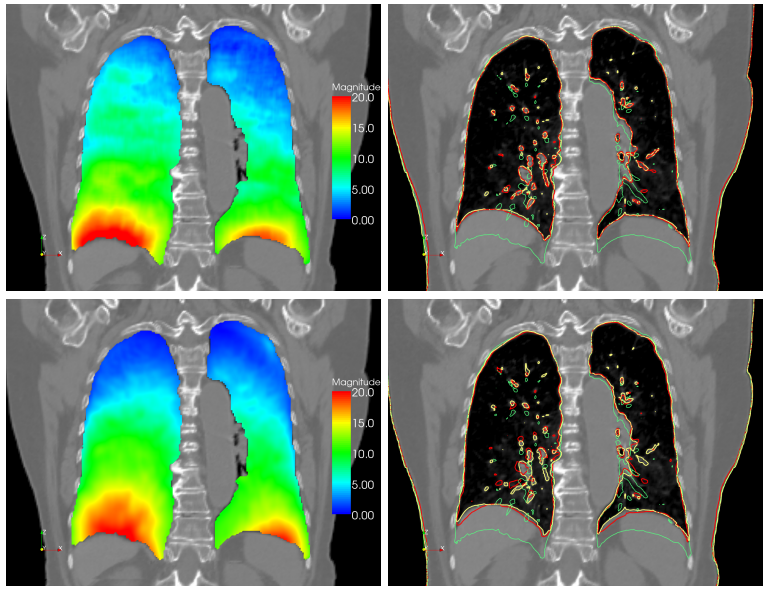

Fig. 2. Result of the motion estimatation by intra–patient registration (top row) and the model–based motion prediction (bottom row) of patient 01. Visualization of the magnitude of the displacement field computed by intra–patient registration (top left) and of the displacement field predicted by the 4D mean motion model (bottom left). Right: contours at end inspiration (green), end expiration (yellow) and estimated/predicted contours at end expiration (red).

The aim of the model generation is to create a representation of the mean healthy lung motion. In a dynamic MRI study by Plathow et al. [18], tumors with diameter $> 3cm$ were shown to influence respiratory lung dynamics. According to their observations, we divide the lungs into two groups: lungs with *intact* dynamics and lungs with *impaired* motion. Lungs without or with only small tumors (volume $< 14.1cm^3$ or diameter $< 3cm$) are defined as intact. Lungs with large tumors or lungs affected by other diseases (e.g. emphysema) are defined as impaired. According to this partitioning, we have 12 data sets with both lungs intact and 6 data sets with at least one impaired lung. Only data sets with intact lungs are used to generate the 4D–MMM.

3.1 Landmark–based evaluation

Due to the high effort of the manual landmark identification only 10 of the 18 data sets are used for the detailed quantitative landmark–based evaluation. Between 70 and 90 inner lung landmarks (prominent bifurcations of the bronchial tree and the vessel tree) were identified manually in the four breathing phases, about 3200 landmarks in total. An intraobserver variability of $0.9 \pm 0.8mm$ was

Table 1. Landmark motion amplitudes and target registration errors $\overline{R}_{EE}$ for the patients considered (in mm). Values are averaged over all landmarks per lung. Lungs with impaired motion are indicated by a gray text color.

Data set	(Lung)	Landmark motion [mm]	Intra-patient registration TRE [mm]	Model-based prediction TRE [mm]
Patient01	left	4,99 ± 4,84	1,51 ± 1,31	2.43 ± 1,64
	right	7,25 ± 4,47	1,41 ± 0,83	3.97 ± 2,08
Patient02	left	7,09 ± 2,92	2,28 ± 1,73	4.26 ± 1,28
	right	4,21 ± 1,75	1,16 ± 0,61	3.82 ± 1,14
Patient03	left	6,15 ± 2,26	1,38 ± 0,73	3.68 ± 1,31
	right	6,28 ± 2,01	1,78 ± 1,05	3.72 ± 1,37
Patient04	left	6,65 ± 2,56	1,53 ± 0,93	4.01 ± 1,60
	right	6,22 ± 3,52	1,44 ± 0,82	2.28 ± 1,09
Patient05	left	5,77 ± 2,03	1,50 ± 0,80	3.17 ± 1,34
	right	3,18 ± 3,36	1,29 ± 1,04	3.47 ± 1,99
Patient06	left	9,67 ± 8,32	1,64 ± 1,42	5.85 ± 2,65
	right	11,85 ± 7,08	1,60 ± 1,00	4.88 ± 2,02
Patient07	left	8,22 ± 6,52	2,45 ± 2,22	3.99 ± 1,79
	right	4,99 ± 6,65	1,49 ± 1,48	3.35 ± 1,69
Patient08	left	5,78 ± 4,14	1,18 ± 0,57	3.15 ± 1,70
	right	6,28 ± 5,63	1,25 ± 1,03	3.11 ± 2,24
Patient09	left	7,43 ± 5,34	1,42 ± 1,22	3.05 ± 1,39
	right	8,41 ± 5,22	1,67 ± 1,03	4.94 ± 3,01
Patient10	left	7,63 ± 5,83	1,93 ± 2,10	3.16 ± 2,29
	right	8,85 ± 6,76	1,76 ± 1,33	5.12 ± 2,34

assessed by repeated landmark identification in all test data sets. The target registration error (TRE) was determined for a quantitative evaluation of the patient–specific registration method and the model–based prediction. The TRE R_j^k is the difference between the motion of landmark k estimated by $\boldsymbol{\varphi}_j$ and the landmark motion as observed by the medical expert.

The mean landmark motion magnitude, i.e. the mean distance of corresponding landmarks, between EI and EE is $6.8 \pm 5.4mm$, ($2.6 \pm 1.6mm$ between EI and ME and $5.0 \pm 2.8mm$ between EI and MI). The TRE of the intra–patient registration is a lower bound for the accuracy of the model–based prediction using the 4D–MMM. The average TRE $\overline{R}_{EE}$ between the reference phase (EI) and EE for patient 01 to 10 (averaged over all landmarks and patients) is $1.6 \pm 1.3mm$ ($1.5 \pm 0.8mm$ between EI and ME and $1.6 \pm 0.9mm$ between EI and MI). Details for all test data sets are shown in table 1.

For each of the 10 test data sets the 4D–MMM is used to predict landmark motion as described in Sect. 2.3. If both lungs of the test data set are intact, a leave–one–out strategy is applied to ensure that the patient data is not used for the model generation. The change in lung air content ΔV_{air} needed for the computation of the scaling factor λ was calculated from the CT images I_{EI} and I_{EE} for each lung side and each test data set. The same factor λ was used to

scale the predicted motion fields $\hat{\varphi}_{EE}$, $\hat{\varphi}_{ME}$ and $\hat{\varphi}_{MI}$. Besides ΔV_{air} no 4D information is used for the model–based prediction.

In Fig. 2 the motion field predicted by the 4D–MMM is compared to the motion field computed by patient–specific registration. A good correspondency between the motion fields is visible, except in the right upper lobe where small deviations occur. The prediction accuracy is illustrated by overlayed contours.

The average TREs $\overline{R}_{EE}$ are listed in table 1 for each of the test data sets and for both the patient–specific and model–based motion estimation. Lungs with impaired motion are indicated by a gray text color. Regarding table 1, lungs with impaired motion generally show higher TREs for the model–based prediction than intact lungs. The average TRE $\overline{R}_{EE}$ for intact lungs is $3.3 \pm 1.8mm$, which is significantly lower ($p < 0.01$) than for lungs with impaired motion ($\overline{R}_{EE} = 4.2 \pm 2.2mm$). Significance is tested by applying a multilevel hierarchical model with the individual R^k values nested within the patient (software: SPSS v.17); data are logarithmized to ensure normal distribution and the model is adjusted to landmark motion.

3.2 Model-based prediction of tumor motion

For a second evaluation of the model, we use expert generated tumor segmentations in two breathing phases (EI and EE) of 9 patient data sets with solid lung tumors. The 4D–MMM is transformed into the coordinate space of each test data set (see Sect. 2.3) and then used to warp the expert–generated tumor segmentation at maximum exhale towards maximum inhale. The distance between the predicted tumor mass center and the center of the manual segmentation was used to evaluate the accuracy of the model–based prediction. Corresponding results are summarized in table 2. Large tumors with a diameter $> 3cm$ are marked in the table as "large".

Regarding table 2 accuracy of the model–based predicted motion of the tumor mass center from EI to EE ranges from $0.66mm$ to $7.38mm$. There is no significant correlation between the tumor motion amplitude and the accuracy of the model-based predicted mass center ($r = 0.19$, $p > 0.15$). Furthermore, it cannot be shown that the prediction accuracy for small tumors is significantly better than for large tumors ($p > 0.4$). In contrast, the model–based prediction accuracy of non-adherent tumors is significantly better than for tumors adhering to chest wall or hilum ($p < 0.05$). In these cases the model presumes the tumour moves like surrounding lung tissue, whereas it rather moves like the adjacent non-lung structure (e.g. chest wall or hilum). In the last column in table 2 those tumors are tagged. Significance is tested by applying a linear mixed model (software: SPSS v.17) and the model is adjusted to tumor motion.

4 Discussion

In this paper, we proposed a method to generate an inter–subject statistical model of the breathing motion of the lung, based on individual motion fields

Table 2. Tumor size and motion amplitude, and the center distances between manually segmented tumor and predicted tumor position (see text for details).

Data set	(Lung)	Tumor size [cm^3]	Tumor motion [mm]	Intra–patient registration TRE [mm]	Model–based prediction TRE [mm]	large	adhere
Patient 01	right	6.5	12.20	0.45	3.54		
Patient 02	right	7.6	2.15	1.44	3.90		X
Patient 03	left	12.7	6.74	0.41	3.91		X
Patient 05	right	8.2	2.34	1.95	5.39		X
	right	17.3	1.68	1.05	4.44	X	X
Patient 06	left	3.4	19.78	2.12	6.87		
	right	128.2	13.78	0.97	2.99	X	
Patient 07	right	2.8	1.31	0.42	0.66		
Patient 08	right	18.4	6.24	0.90	1.59	X	
Patient 09	right	88.9	8.35	0.29	5.33	X	X
Patient 10	right	96.1	1.77	1.01	7.46	X	X

extracted from 4D CT images. Methods to apply this model in order to predict patient–specific breathing motion without knowledge of 4D image information were presented. Ten 4D CT data sets were used to evaluate the accuracy of the image–based motion field estimation and the model–based motion field prediction. The intra–patient registration shows an average TRE in the order of the voxel size, e.g. $1.6 \pm 1.3mm$ when considering motion between EI and EE. The 4D–MMM achieved an average prediction error (TRE) for the motion between EI and EE of $3.3 \pm 1.8mm$. Regarding that besides the calculated scaling factor λ no patient–specific motion information is used for the model–based prediction and that the intra–patient registration as well as the atlas–patient registration is error prone, we think this is a promising result. Thus we believe that a statistical respiratory motion model has the capability of providing valuable prior knowledge in many fields of applications.

Since the statistical model represents intact respiratory dynamics, it was shown that the prediction precision is significantly lower for lungs affected by large tumours or lung disorders ($4.2 \pm 2.2mm$). These results indicate (at least for the 10 lung tumor patients considered) that large tumors considerably influence respiratory lung dynamics. This finding is in agreement with Plathow et al. [18]. In addition, we applied the 4D–MMM to predict patient–specific tumor motion. No correlation between prediction accuracy and tumor size or tumor motion amplitude could be detected (at least for our test data sets). We observed that tumors adhering to non–lung structures degrade local lung dynamics significantly and model–based prediction accuracy is decreased for these cases.

To conclude this paper, we present two examples of possible applications of the statistical respiratory motion model.

Application examples: The capability of the 4D–MMM to predict tumor motion for radiotherapy planning is exemplarily illustrated for patient 01. This patient has a small tumor not adherent to another structure, and a therapeutically

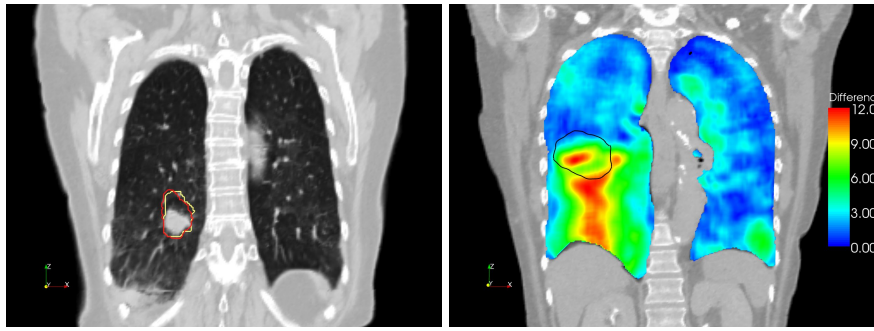

(a) (b)

Fig. 3. (a) Visualization of the internal target volume (ITV) of patient 01 in a coronal CT slice. The ITV was calculated from expert-defined tumor segmentations (yellow contour) and from tumor positions predicted by the average motion model (red contour). (b) Visualization of the difference between lung motion estimated by patient–specific registration and lung motion predicted by the 4D–MMM for patient 09. The left lung shows intact lung motion; dynamics of the right lung are impaired by the large tumor. The contour of the tumor is shown in black.

relevant tumor motion of 12.2mm. An important measure for planning in 3D conformal radiotherapy is the internal target volume (ITV), which contains the complete range of motion of the tumour. For this patient, the ITV is calculated first from expert-defined tumor segmentations in the images acquired at EI, EE, ME and MI. In a second step, the expert segmentation in EI is warped to EE, ME and MI using the 4D–MMM and the ITV is calculated based on the warped results. The outlines of both ITVs are shown in Fig. 3(a).

A second example demonstrates that the 4D–MMM could be helpful from the perspective of image-guided diagnosis. Here, the motion pattern of individual patients are compared to a "normal" motion, represented by the 4D–MMM. To visualize the influence of a large tumor to the respiratory motion, the difference between the individual motion field computed by intra–patient registration and the motion field predicted by the 4D–MMM is shown in Fig. 3(b). The left lung shows differences of only about 3mm, whereas the large differences to the intact lung motion indicate that the respiratory dynamics of the right lung are influenced by the large tumor.

Currently, the statistical motion model represents the average motion in the training population. A main focus of our future work is to include the variability of the motion into the model. Here, the Log–Euclidean framework provides a suitable technique for more detailed inter–patient statistics.

References

1. Keall, P.J., Mageras, G., Balter, J.M., et al.: The management of respiratory motion in radiation oncology report of AAPM task group 76. Med Phys **33**(10)

(2006) 3874–3900
2. Vik, T., Kabus, S., von Berg, J., Ens, K., Dries, S., Klinder, T., Lorenz, C.: Validation and comparison of registration methods for free-breathing 4D lung CT. In: SPIE Medical Imaging 2008. Volume 6914., SPIE (2008) 2P
3. Werner, R., Ehrhardt, J., Schmidt-Richberg, A., Handels, H.: Validation and comparison of a biophysical modeling approach and non-linear registration for estimation of lung motion fields in thoracic 4D CT data. In: SPIE Medical Imaging 2009: Image Processing. Volume 7259. (2009) 0U–1–8
4. Werner, R., Ehrhardt, J., Schmidt, R., Handels, H.: Patient-specific finite element modeling of respiratory lung motion using 4D CT image data. Med Phys **35**(5) (May 2009) 1500–1511
5. Arsigny, V.: Processing Data in Lie Groups: An Algebraic Approach. Application to Non-Linear Registration and Diffusion Tensor MRI. Thèse de sciences (phd thesis), École polytechnique (November 2006)
6. Li, B., Christensen, G.E., Hoffman, E.A., McLennan, G., Reinhardt, J.M.: Establishing a normative atlas of the human lung: intersubject warping and registration of volumetric CT images. Acad Radiol **10** (2003) 255–265
7. Segars, W., Lalush, D., Tsui, B.: Modeling respiratory mechanics in the MCAT and spline-based MCAT phantoms. IEEE Trans Nucl Sci **48**(1) (Feb 2001) 89–97
8. Sundaram, T.A., Avants, B.B., Gee, J.C.: A dynamic model of average lung deformation using capacity-based reparameterization and shape averaging of lung mr images. In: MICCAI 2004, Springer (2004) 1000–1007
9. Klinder, T., Lorenz, C., Ostermann, J.: Respiratory motion modeling and estimation. In: Workshop on Pulmonary Image Analysis, New York, USA (2008) 53–62
10. Ehrhardt, J., Werner, R., Schmidt-Richberg, A., Schulz, B., Handels, H.: Generation of a mean motion model of the lung using 4D CT data. In: Visual Computing for Biomedicine, Delft, Eurographics Association (2008) 69–76
11. Ehrhardt, J., Werner, R., Säring, D., Frenzel, T., Lu, W., Low, D., Handels, H.: An optical flow based method for improved reconstruction of 4D CT data sets acquired during free breathing. Med Phys **34**(2) (Feb 2007) 711–721
12. Miller, M.I.: Computational anatomy: shape, growth, and atrophy comparison via diffeomorphisms. NeuroImage **23 Suppl 1** (2004) S19–S33
13. Vercauteren, T., Pennec, X., Perchant, A., Ayache, N.: Symmetric log-domain diffeomorphic registration: a demons-based approach. In: Med Image Comput Comput Assist Interv, MICCAI 2008, Springer (2008) 754–761
14. Beg, M.F., Miller, M.I., Trouve, A., Younes, L.: Computing large deformation metric mappings via geodesic flows of diffeomorphisms. Int J Comp Vis **61**(2) (2005) 139–157
15. Arsigny, V., Commowick, O., Pennec, X., Ayache, N.: A log-Euclidean framework for statistics on diffeomorphisms. In: MICCAI 2006, Springer (2006) 924–931
16. Bossa, M.N., Gasso, S.O.: A new algorithm for the computation of the group logarithm of diffeomorphisms. In: MFCA 2008, New York, USA (2008)
17. Lu, W., Parikh, P.J., El Naqa, I.M., et al.: Quantitation of the reconstruction quality of a four-dimensional computed tomography process for lung cancer patients. Med Phys **32** (2005) 890–901
18. Plathow, C., Fink, C., Ley, S., M.Puderbach, M.Eichinger, I.Zuna, A.Schmähl, H.Kauczor: Measurement of tumor diameter-dependent mobility of lung tumors by dynamic MRI. Radiother Oncol **73** (2004) 349–354